Communication

Stable High-Gain Linearly and Circularly Polarized Dielectric Resonator Antennas Based on Multiple High-Order Modes

Lin Wang, Sai-Wai Wong, Xiao Zhang, Yejun He, Long Zhang, Wenting Li, and Lei Zhu

***Abstract*— Dielectric resonator antennas (DRAs) under high-order multiple-modes resonator (MMR) for stable high gain are proposed in this communication. The approach is to implement slot cuts on the surface of DR for reconstructing the electric field distribution of high-order resonance modes. In this way, the sidelobes are reduced and two high-order modes are reallocated to construct a continuous wide band. Various MMR configurations were proposed in this work. First, a DRA operating in TE^x_{031} and TE^x_{051} modes is proposed with a pair of loaded slots to realize a fractional bandwidth (FBW) of 26% and a stable gain as high as 8.3 dBi within the desired passband. Second, a DRA with TE^x_{051} and TE^x_{071} modes is developed by introducing two pairs of slots, and an impedance FBW of 12.8% and a stable gain as high as 11 dBi are achieved. Third, three pairs of slots are introduced to the DRA with TE^x_{091} and $TE^x_{0,11,1}$ modes, and an impedance FBW of 6.4% and a stable antenna gain as high as 12.3 dBi are obtained. At last, a circularly polarized (CP) DRA array with four proposed linearly polarized (LP) DRA elements is designed with an impedance bandwidth of 51.8%, a 3 dB axial-ratio (AR) FBW of 32%, a peak gain of 13.89 dBic, and a 1 dB gain bandwidth of 19.9%.**

***Index Terms*— Circular polarization, dielectric resonator antennas (DRAs), high-order modes, slots, stable high gain.**

I. Introduction

Dielectric resonator antennas (DRAs) have been extensively appreciated as radiating elements since first proposed [1]. Because of several advantageous properties compared to other radiating elements, such as less conductive loss at higher frequencies, high radiation efficiency [2], high degree of design flexibility, and their ease of excitation modes, DRAs have become a very good choice for wireless communications. However, conventional DRAs commonly have a relatively low gain of about 5 dBi, which is below the requirement in some specific application scenarios. To combat path loss of far-range propagation, the communication systems require that antennas must be high-gain. Otherwise, antennas with low gain will lead to a reduced signal-to-noise ratio and ask for higher sensitivity of receivers.

There have been several methods introduced to enhance the gain of DRAs in [3], [4], [5], [6], [7], [8], [9], [10], [11], [12], [13], [14], [15], [16], [17], [18], [19], [20], [21], [22], and [23]. Among these methods, the most widely used method is DRA array design [3], [4], [5], [6], [7], [8], [9], [10], [11], [12]. However, these high-gain array designs require a number of power dividers, which will inevitably increase the complexity and loss of the feeding network.

Manuscript received 28 April 2022; revised 8 August 2022; accepted 26 August 2022. Date of publication 30 September 2022; date of current version 22 December 2022. This work was supported in part by the National Natural Science Foundation of China under Grant 62171289, Grant 81771955, Grant 61861022, and Grant 62071306; and in part by the Shenzhen Science and Technology Programs under Grant JCYJ 20190728151457763. *(Corresponding author: Xiao Zhang.)*

Lin Wang, Sai-Wai Wong, Xiao Zhang, Yejun He, Long Zhang, and Wenting Li are with the College of Electronics and Information Engineering, Shenzhen University, Shenzhen 518060, China (e-mail: xiao.zhang@szu.edu.cn).

Lei Zhu is with the Department of Electrical and Computer Engineering, Faculty of Science and Technology, University of Macau, Macao, China.

Color versions of one or more figures in this communication are available at https://doi.org/10.1109/TAP.2022.3209627.

Digital Object Identifier 10.1109/TAP.2022.3209627

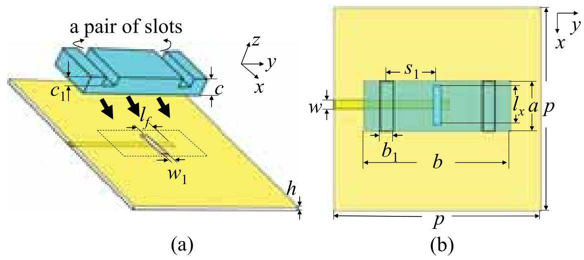

Fig. 1. Geometrical configuration of antenna A. (a) 3-D view. (b) Top view. Design parameters: $p = 92$, $h = 1$, $l_f = 9.1$, $w = 2.1$, $l_x = 22.5$, $w_1 = 3$, $a = 21$, $b = 65$, $c = 8.32$, $b_1 = 6.76$, $c_1 = 4.68$, $s_1 = 21.3$ (unit: mm).

There have been other methods introduced to enhance gain of DRAs in [13], [14], [15], [16], [17], [18], [19], [20], [21], [22], and [23]. In [13], a hybrid DRA increases the gain by 3 dB through a mushroom-like electromagnetic band-gap (EBG) structure, which suppresses the propagation of lateral surface waves. Another design approach is to increase the radiation from the side walls of the DRA. In [14], a peak gain of 9.6 dBi has been realized with the fundamental mode by engraving grooves on the side walls. Besides, stacked dielectric layers also have been proved to be an effective method for enhanced gain in [16] and [17]. At last, high-order modes are also utilized to increase the gain of DRAs in [18], [19], [20], [21], [22], and [23]. In [18], by exciting the high-order modes, the antenna gain can be enhanced by 5 dB as compared with the fundamental mode. It is confirmed that high-order modes possess higher potential in the enhancement of gain as compared with the fundamental mode because the DRAs have a larger radiation area. However, the potential of gain enhancement for DRAs has not been fully excavated in these reported works, and the impedance bandwidth and 3 dB gain bandwidth of DRAs are still narrow [18], [19], [20], [21], [22], [23].

In this communication, an electric field reshaping and slot-loading [24], [25], [26], [27] method is developed to improve the radiation performance and bandwidth of high-order-modes DRAs. This design method turns unusable modes into usable modes. The working principle is demonstrated and verified through three design examples, i.e., antenna A, B, and C, which operate in TE^x_{031}/TE^x_{051}, TE^x_{051}/TE^x_{071}, and TE^x_{091}/$TE^x_{0,11,1}$ modes, respectively. It is noteworthy that, those three proposed stable high-gain multiple-modes resonator (MMR) antennas were constructed in a single DRA structure without any power divider. At last, four elements developed from antenna B are utilized to construct a circularly polarized (CP) DRA array, whose gain is much higher than that of the conventional array.

II. Three Antenna Designs

A. Antenna A Working in TE^x_{031} and TE^x_{051} Modes

Fig. 1(a) and (b) shows the 3-D view and the top view, respectively, of the first DRA design named antenna A operating in TE^x_{031} and

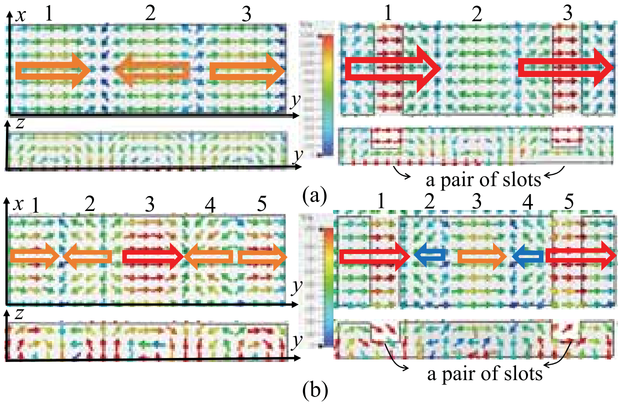

Fig. 2. Simulated E-field distribution of two modes with and without slots. (a) TE^x_{031} mode. (b) TE^x_{051} mode.

TE^x_{051} modes. The antenna consists of a dielectric resonator and a feed network. The dielectric resonator is a rectangular ceramic block with relative permittivity of $\varepsilon_r = 12$ and a loss tangent of 0.0002, and two symmetrical rectangular slots are cut out from the upper side. The feeding network is printed on an F4BM substrate with a thickness of 1 mm, the relative permittivity of 2.65, and loss tangent of 0.0015.

The radiation pattern produced by TE^x_{031} mode of the rectangular DRA is usually unusable because the sidelobe level (SLL) is too high. This can be explained with the E-field distribution of TE^x_{031} mode. In Fig. 2(a), the left figure depicts the E-field distribution of TE^x_{031} mode without two slots. Their E-field strength is indicated by color, including red (strong), blue (weak), and orange (medium). Since the phases of the second semi-period of E-field vectors are adverse to those of the first and third semi-periods, their radiation will be canceled out in a specific direction in the far zone and produce a high level of sidelobes. Similarly, as for the TE^x_{051} mode, the phases of the first, third, and fifth semi-periods are adverse to those of the second and fourth semi-periods.

Fakhte *et al.* [14] have discussed the influence of slotting on E-fields of the fundamental mode. When a slot is loaded to the dielectric, the dielectric, the E-field at the slotted position will increase while that at other positions will decrease. According to this principle, it is possible to enhance the desired in-phase E-fields for TE^x_{031} and TE^x_{051} modes and weaken the reversed E-fields, so that the radiation patterns will be improved.

The right figure in Fig. 2(a) shows the E-field distribution of TE^x_{031} when two slots are introduced to the DRA. Apparently, the E-fields of these two semi-periods at two sides are enhanced, and the E-field at the central semi-period is weakened as compared to the case without slots. As for the TE^x_{051} mode, the E-fields of the first and fifth semi-periods are enhanced and the reversed E-fields at other semi-periods are weakened.

Fig. 3 shows the radiation patterns of antenna A with and without a pair of slots. By comparing the radiation patterns under TE^x_{031} mode operation, it can be found that the broadside directivity is enhanced by 3.85 dB and the SLL is reduced by 1.5 dB. As for the TE^x_{051} mode, the broadside directivity is enhanced by 0.415 dB and the SLL is slightly increased among the acceptable range.

The simulated reflection coefficients and realized gain of antenna A are depicted in Fig. 4. It can be found that the TE^x_{031} mode is more sensitive to the slot loading, because slots are at the positions of the semi-periods with the maximum E-field for TE^x_{031} mode. Thus,

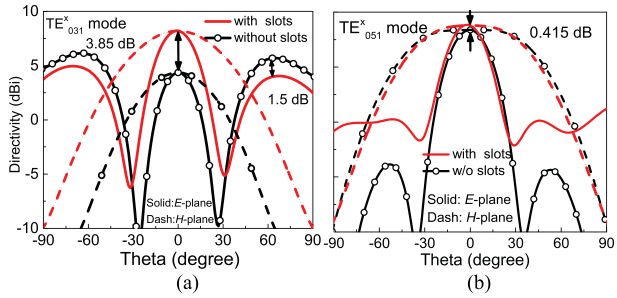

Fig. 3. Radiation patterns with and without slots for two modes. (a) TE^x_{031} mode. (b) TE^x_{051} mode.

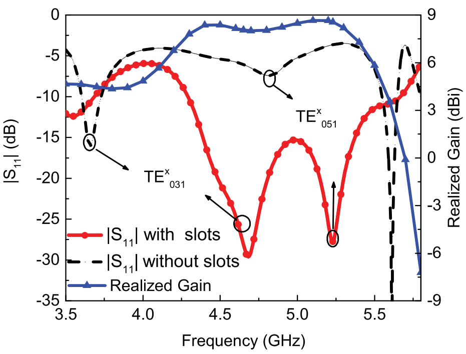

Fig. 4. Simulated results of $|S_{11}|$ and realized gain of antenna A.

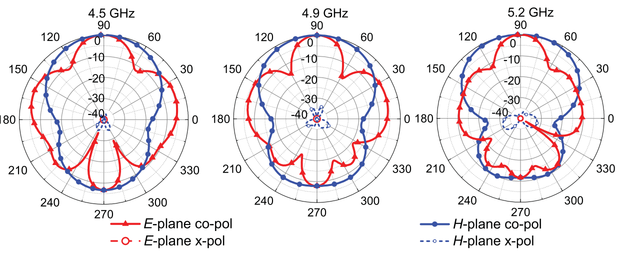

Fig. 5. Simulated radiation patterns of antenna A at 4.5, 4.9, and 5.2 GHz.

the two modes get close to each other after the antenna is cut out with slots. Two reflection zeros come up and produce an impedance bandwidth of 26% (4.3–5.6 GHz). The realized gain response in the band is very flat and stable with little variation, and the gain level is as high as 8.3 dBi. In addition, the simulated radiation patterns of the antenna at 4.5, 4.9, and 5.2 GHz are depicted in Fig. 5. The H-plane radiation patterns are almost the same in simulation at the three frequencies. Though the E-plane SLLs are slightly different, the half-power beamwidths (HPBWs) of the main beams are stable.

B. Antenna B Working in TE^x_{051} and TE^x_{071} Modes

Fig. 6(a) and (b) shows the 3-D view and the top view, respectively, of the second DRA named antenna B which operates in TE^x_{051} and TE^x_{071} modes. The feed part is similar to the last design in Fig. 1, and the same substrate and ceramic for DRA are used as default. The difference is that the rectangular ceramic block was cut out with two pairs of symmetrical rectangular slots.

In this design, slots are loaded to reshape the E-field distribution of the two operating modes and reallocate the frequencies of TE^x_{051} and TE^x_{071} modes, which aim to achieve higher stable gain and a continuous wide band as desired.

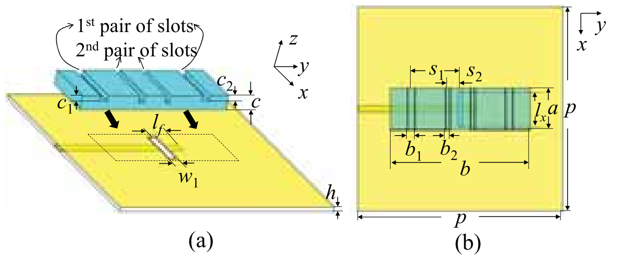

Fig. 6. Geometrical configuration of antenna B. (a) 3-D view. (b) Top view. Design parameters: $p = 107$, $h = 1$, $l_f = 8.8$, $w = 3.7$, $l_x = 20$, $w_1 = 1.8$, $a = 21.4$, $b = 73$, $c = 7.3$, $b_1 = 3.8$, $c_1 = 2.8$, $s_1 = 25.5$, $b_2 = 2.4$, $c_2 = 3.7$, $s_2 = 6$ (unit: mm).

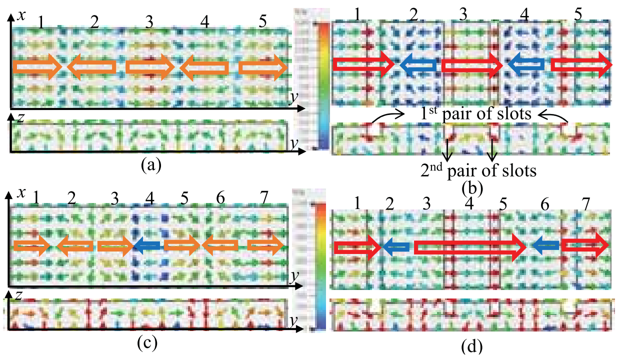

Fig. 7. Simulated E-field distribution of the two modes with and without slots. (a) TE^x_{051} mode without slots. (b) TE^x_{051} mode with slots. (c) TE^x_{071} mode without slots. (d) TE^x_{071} mode with slots.

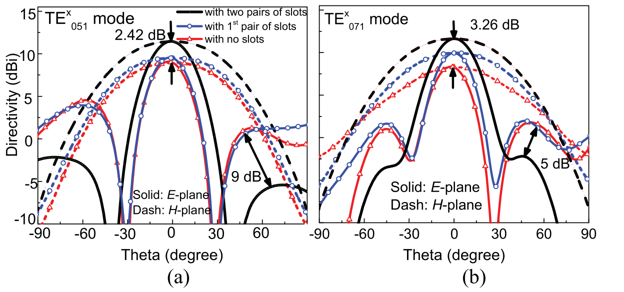

Fig. 8. Radiation patterns of antenna B for two modes under different slot loading conditions. (a) TE^x_{051} mode. (b) TE^x_{071} mode.

First, the E-fields of the TE^x_{051} and TE^x_{071} modes without slots are investigated in Fig. 7(a) and (c), respectively. Fig. 7(b) and (d) shows the E-fields of the two modes after the slots are loaded. As for the case with TE^x_{051} mode, the E-fields of the first, third, and fifth semi-periods are enhanced, and the reversed E-fields of the second and fourth semi-periods are attenuated. Similarly, the E-fields of the first, third, fifth, and seventh semi-periods of TE^x_{071} mode are enhanced, and the reversed E-fields are suppressed.

The radiation patterns of antenna B with different slot-loading schemes are investigated in Fig. 8. As the number of slots increases, the broadside directivity for the two modes is gradually increased. When the two pairs of slots are loaded, the SLL for TE^x_{051} mode is reduced by 9 dB, and consequently, the broadside directivity is enhanced by 2.42 dB. As for the TE^x_{071} mode, the SLL is reduced by 5 dB, and broadside directivity is enhanced by 3.26 dB as a result.

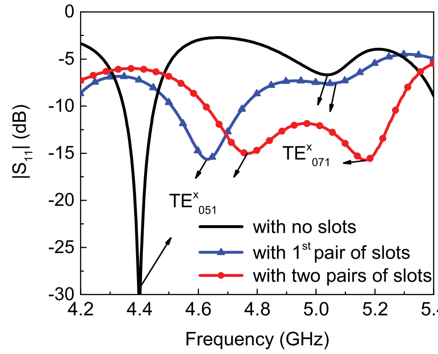

Fig. 9. Reflection coefficients of antenna B under different slot loading schemes.

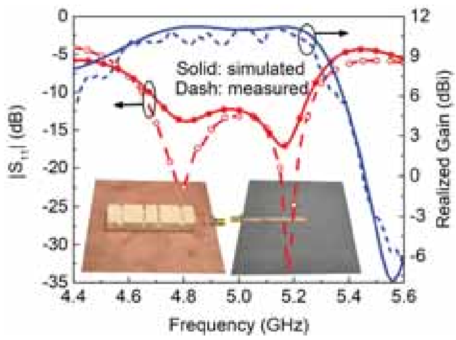

Fig. 10. Simulated and measured $|S_{11}|$ and realized gain of antenna B.

The reflection coefficients of the antenna under different slot loading schemes are shown in Fig. 9. It is found that the transmission pole accounting for TE^x_{051} mode approaches that for TE^x_{071} mode when the first pair of slots is loaded. When the two pairs of slots are both introduced, the two poles are slightly moved to high frequency and the matching is well improved.

Fig. 10 shows the simulated and measured reflection coefficients and realized gain of antenna B. The simulated and measured 10 dB return-loss bandwidths are 12.3% (4.67–5.28 GHz) and 12.8% (4.65–5.29 GHz), respectively. The realized gain response in the band is very flat and stable, and the gain level is as high as 11 dBi. The measured and simulated radiations patterns at 4.75 and 5.15 GHz are shown in Fig. 11. The radiations patterns are almost the same at the two frequencies.

C. Antenna C Working in TE^x_{091} and $TE^x_{0,11,1}$ Modes

The previous designs have demonstrated that the proposed method is useful for TE^x_{0n1} modes of the rectangular DRA, where $n = 3$, 5, and 7. It is questionable whether modes with higher order can be utilized to achieve higher gain. To answer this question, a DRA working in TE^x_{091} and $TE^x_{0,11,1}$ modes is proposed and designed.

Fig. 12(a) and (b) shows the 3-D view and the top view, respectively, of the third DRA named antenna C operating in TE^x_{091} and $TE^x_{0,11,1}$ modes. The rectangular ceramic block is cut out with three pairs of symmetrical rectangular slots.

First, the E-field distribution of TE^x_{091} mode with and without the three pairs of slots is investigated in Fig. 13(a) and (b), respectively. It can be found that the desired in-phase E-fields of the first, third, fifth, seventh, and ninth semi-periods of the TE^x_{091} mode are enhanced, while the unwanted out-of-phase E-fields at other semi-periods are restrained. Similarly, as shown in Fig. 13(c) and (d)

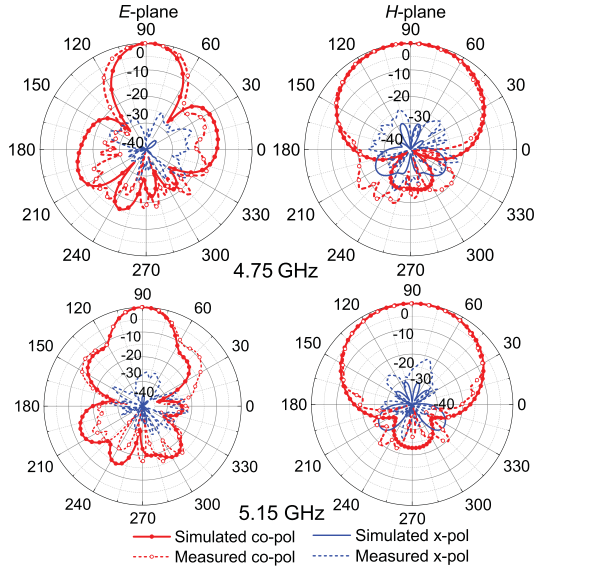

Fig. 11. Simulated and measured radiation patterns at 4.75 and 5.15 GHz.

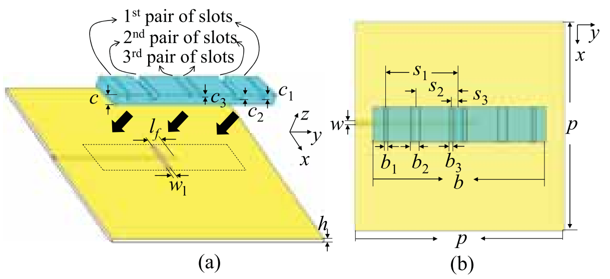

Fig. 12. Geometrical configuration of antenna C. (a) 3-D view. (b) Top view. Design parameters: $p = 160$, $h = 1$, $l_f = 15$, $w = 0.8$, $l_x = 14.5$, $w_1 = 1$, $a = 24$, $b = 120$, $c = 8.2$, $b_1 = 2.3$, $c_1 = 3.9$, $s_1 = 50.6$, $b_2 = 6$, $c_2 = 4.2$, $s_2 = 31.8$, $b_3 = 2$, $c_3 = 2.6$, $s_3 = 4.2$ (unit: mm).

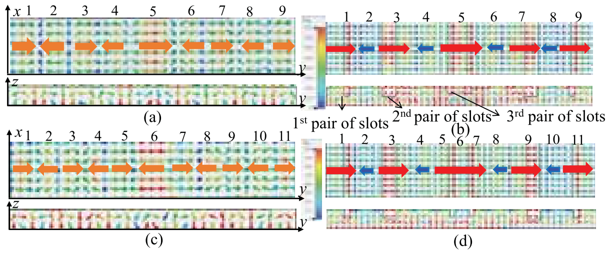

Fig. 13. Simulated E-field distribution of the two modes with and without slots. (a) TE^x_{091} mode without slots. (b) TE^x_{091} mode with slots. (c) $\text{TE}^x_{0,11,1}$ mode without slots. (d) $\text{TE}^x_{0,11,1}$ mode with slots.

for $\text{TE}^x_{0,11,1}$ mode, the desired in-phase E-fields of the 1st, 3rd, 5th, 7th, 9th, and 11th semi-periods are enhanced, while other unwanted out-of-phase E-fields semi-periods are restrained.

As shown in Fig. 14, due to the reshaped E-field distribution, the E-plane SLL of the antenna under TE^x_{091} mode operation is reduced by 7.5 dB when the six slots are introduced, and thus the broadside directivity is enhanced by 5.32 dBi. Similarly, as for the $\text{TE}^x_{0,11,1}$ mode, the E-plane SLL is reduced by 5.32 dB and the broadside directivity is enhanced by 11.15 dB.

Next, the simulated reflection coefficients and realized gain of antenna C are investigated in Fig. 15. As compared with the antenna

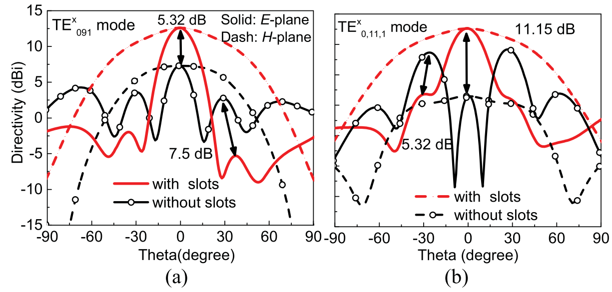

Fig. 14. Radiation patterns of antenna C with and without slots for two modes. (a) TE^x_{091} mode. (b) $\text{TE}^x_{0,11,1}$ mode.

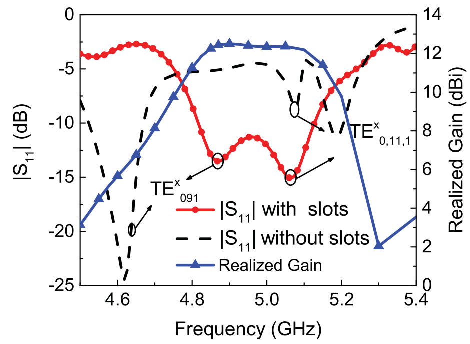

Fig. 15. Simulated $|S_{11}|$ and realized gain of antenna C.

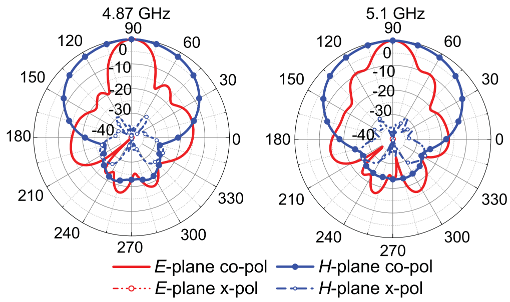

Fig. 16. Simulated radiation patterns of antenna C at 4.87 and 5.1 GHz.

without slots, the resonant frequencies of TE^x_{091} and $\text{TE}^x_{0,11,1}$ modes of the slot-loaded antenna C become closer to each other. A 6.4% (4.87–5.13 GHz) bandwidth of 10 dB return-loss is achieved. The realized-gain response in the band is flat and stable with little variation, and the average gain is up to 12.3 dBi.

The simulated radiation patterns of the antenna prototype at the frequencies of 4.87 and 5.1 GHz are shown in Fig. 16. The front-to-back ratio of the antenna is over 22 dB, and the co-polarization to cross-polarization ratio is over 35 dB.

D. Discussion

In Table I, the performance of the three proposed antennas is compared with other DRAs based on higher-order modes in [18], [19], [20], [21], [22], and [23] and conventional DRA array in [11] and [12]. It can be seen that the proposed antennas are advantageous in impedance bandwidth, profile, and gain as compared with those in [18], [19], [20], [21], and [22]. In [23], the impedance bandwidth is enhanced to 21%, but the gain stability is very poor. And compared to the four-element conventional arrays in [11] and [12], the greatest advantage of our proposed antennas is to achieve a similar high

TABLE I
PERFORMANCE COMPARISON WITH REPORTED WORKS

Ref	BW (%)	Max. gain_ (dBi)	Antenna height (λ)
[18]	8.3	10	1.1
[19]	narrow	8.5	0.35
[20]	narrow	9.5	0.35
[21]	2.6	11.6	0.47
[22]	2.6	9.12	0.55
[23]	21	11	1.53
[11]	12	10.5	0.134
[12]	4.7	11.7	0.234
antenna A	26	8.3 (average)	0.138
antenna B	12.8	11 (average)	0.138
antenna C	6.4	12.3 (average)	0.153

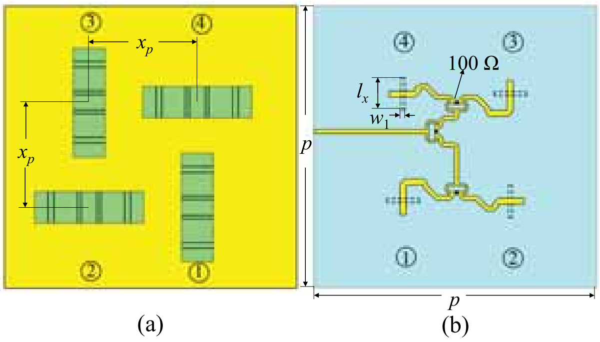

Fig. 17. Geometrical configuration of the CP DRA array. (a) Top view. (b) Bottom view. Design parameters: $p = 180$, $x_p = 34$, $l_x = 20$, $w_1 = 1.8$ (unit: mm).

gain only in a single DRA structure without any power divider. For example, the array in [11] achieves a maximum gain of about 10.5 dBi, but it consists of four DRA elements, which also require additional power dividing networks.

As compared with antenna B, the bandwidth of antenna C gets a little narrower, because the radiation quality factor is increased when the mode order becomes higher. Besides, the gain enhancement of antenna C is less significant because the number and level of sidelobes are increased, and the ground size is not optimal.

III. CP DRA ARRAY

Four linearly polarized (LP) DRAs can generate CP fields by feeding them with a 90° phase difference and equal amplitude. Fig. 17 shows the top view and the bottom view. The high-gain antenna element, which is developed from antenna B, is employed to construct a sequential array as depicted in Fig. 17(a).

The reflection coefficient and axial-ratio (AR) results, as well as the photograph of the antenna, are shown in Fig. 18. The simulated and measured 10 dB return-loss bandwidths are 51.8% (3.2–5.44 GHz) and 44.4% (3.5–5.5 GHz), and the simulated and measured 3 dB AR bandwidths are 32% (3.82–5.31 GHz) and 22.5% (4.18–5.24 GHz), respectively. The reason for the difference between the simulated and measured AR bandwidths may be the errors in matching and phase caused by feeding networks.

Fig. 19 shows the realized gains and directivity of the CP DRA array and antenna B element. The maximum gain of the CP array is 13.89 dBic at 5.04 GHz. It is interesting that the 1 dB gain bandwidth of 19.9% for this CP DRA array is wider than the 12.3% fractional bandwidth (FBW) of the antenna B element. This is because the radiation performance at low frequency has been improved. Such directivity improvement is mainly caused by the

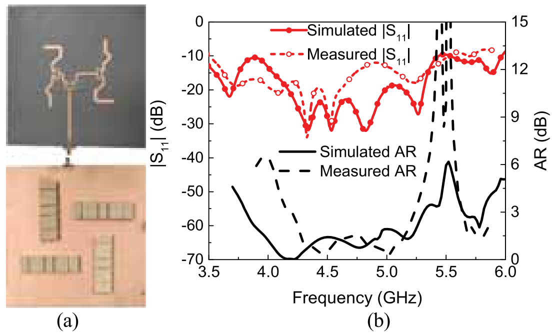

Fig. 18. Photograph of the CP DRA array and its results of reflection coefficient and AR. (a) Photograph. (b) Reflection coefficient and AR.

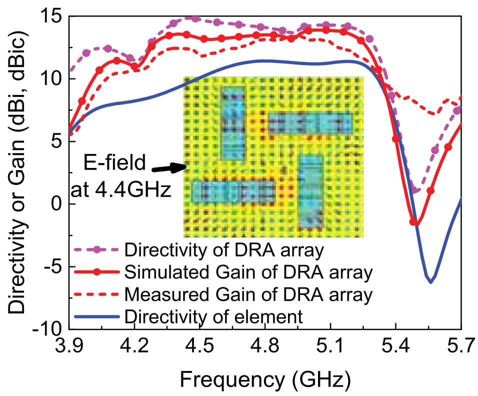

Fig. 19. Directivity and gain results of the CP DRA array and antenna B element.

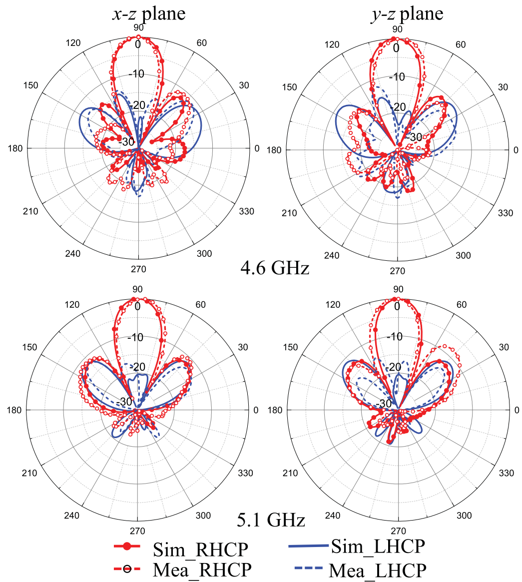

Fig. 20. Radiation patterns at 4.6 and 5.1 GHz.

coupling effect between antenna elements. The E-field distribution of CP DRA at 4.4 GHz is shown in Fig. 19. It can be found that the coupling E-field between elements is quite strong, and it enhances the aperture efficiency. Fig. 20 shows the radiation patterns in the xz- and xy-planes at 4.6 and 5.1 GHz. The HPBWs are much

TABLE II

PERFORMANCE COMPARISON WITH REPORTED WORKS

Ref.	Radiators	Imp. BW (%)	AR BW (%)	Dividers	Max. gain (dBic)	1-dB gain BW (%)
[4]	16	2.4	2.4	15	16	2.4
[5]	8	52	42.9	7	12.5	narrow
[6]	8	25.1	21.4	3	15.1	17.3
[7]	4	19.3	10.4	7	13.6	19
[8]	4	>15.9	15.9	3	11.43	4.9
[9]	4	30.9	23.52	3	10	9.8
[10]	4	25.9	21.3	3	15.5	6.4
This work	4	51.8	32	3	13.89	19.9

narrower than those of the conventional four-element arrays and so high gain can be obtained.

To highlight the contribution of this work, a performance comparison is made with the reported CP DRA arrays in Table II. In general, the proposed CP DRA array has a wider 1 dB gain bandwidth, showing a much steadier gain response. As compared with the arrays in [4], [5], [6], and [7], our proposed antenna can achieve comparable gain with fewer power dividers or radiators. As compared with the array in [8] and [9], our proposed antenna can achieve higher gain with the same number of radiators and power dividers. As compared with the high-gain array in [10], the achieved impedance bandwidth and 1 dB gain bandwidth in this work are much wider.

IV. CONCLUSION

An electric field reshaping and slot-loading method is proposed to improve the radiation performance and bandwidth of high-order modes of DRAs. First, three DRA designs, i.e., antennas A, B, and C, under different selections of high-order modes were studied to achieve stable higher antenna gain without using traditional multi-antenna elements. Next, a CP DRA array based on antenna B is designed, and the coupling between elements contributes to wider 1 dB gain bandwidth. The proposed antennas have the advantages of enhanced bandwidth and stable high gain.

REFERENCES

[1] S. Long, M. McAllister, and L. C. Shen, “The resonant cylindrical dielectric cavity antenna,” *IEEE Trans. Antennas Propag.*, vol. AP-31, no. 3, pp. 406–412, May 1983.

[2] Q. Lai, G. Almpanis, C. Fumeaux, H. Benedickter, and R. Vahldieck, “Comparison of the radiation efficiency for the dielectric resonator antenna and the microstrip antenna at Ka band,” *IEEE Trans. Antennas Propag.*, vol. 56, no. 11, pp. 3589–3592, Nov. 2008.

[3] P. R. Meher, B. R. Behera, S. K. Mishra, and A. A. Althuwayb, “A chronological review of circularly polarized dielectric resonator antenna: Design and developments,” *Int. J. RF Microw. Comput.-Aided Eng.*, vol. 31, no. 5, May 2021, Art. no. e22589.

[4] L. Lu, Y.-C. Jiao, Z.-B. Weng, L. Zhang, C.-Y. Cui, and R.-Q. Wang, “High-efficiency circularly polarized dielectric resonator antenna array fed by the cavity-backed SIW,” *IEEE Antennas Wireless Propag. Lett.*, vol. 17, no. 7, pp. 1145–1148, Jul. 2018.

[5] W.-W. Liu, Z.-H. Cao, and Z. Wang, “A wideband circularly polarized dielectric resonator antenna array,” *IEEE Access*, vol. 9, pp. 99589–99594, 2021.

[6] W.-W. Yang, W.-J. Sun, H. Tang, and J.-X. Chen, “Design of a circularly polarized dielectric resonator antenna with wide bandwidth and low axial ratio values,” *IEEE Trans. Antennas Propag.*, vol. 67, no. 3, pp. 1963–1968, Mar. 2019.

[7] B. Rana and S. K. Parui, “Microstrip line fed wideband circularly-polarized dielectric resonator antenna array for microwave image sensing,” *IEEE Sensors Lett.*, vol. 1, no. 3, pp. 1–4, Jun. 2017.

[8] Y.-X. Sun and K. W. Leung, “Circularly polarized substrate-integrated cylindrical dielectric resonator antenna array for 60 GHz applications,” *IEEE Antennas Wireless Propag. Lett.*, vol. 17, no. 8, pp. 1401–1405, Aug. 2018.

[9] S. Gupta, A. Sharma, G. Das, R. K. Gangwar, and M. Khalily, “Wideband circularly polarized dielectric resonator antenna array with polarization diversity,” *IEEE Access*, vol. 7, pp. 49069–49076, 2019.

[10] W.-J. Sun, W.-W. Yang, P. Chu, and J.-X. Chen, “Design of a wideband circularly polarized stacked dielectric resonator antenna,” *IEEE Trans. Antennas Propag.*, vol. 67, no. 1, pp. 591–595, Jan. 2019.

[11] A. A. Qureshi, D. M. Klymyshyn, M. Tayfeh, W. Mazhar, M. Borner, and J. Mohr, “Template-based dielectric resonator antenna arrays for millimeter-wave applications,” *IEEE Trans. Antennas Propag.*, vol. 65, no. 9, pp. 4576–4584, Sep. 2017.

[12] W. M. Abdel-Wahab, D. Busuioc, and S. Safavi-Naeini, “Millimeter-wave high radiation efficiency planar waveguide series-fed dielectric resonator antenna (DRA) array: Analysis, design, and measurements,” *IEEE Trans. Antennas Propag.*, vol. 59, no. 8, pp. 2834–2843, Aug. 2011.

[13] T. A. Denidni, Y. Coulibaly, and H. Boutayeb, “Hybrid dielectric resonator antenna with circular mushroom-like structure for gain improvement,” *IEEE Trans. Antennas Propag.*, vol. 57, no. 4, pp. 1043–1049, Apr. 2009.

[14] S. Fakhte, H. Oraizi, and L. Matekovits, “Gain improvement of rectangular dielectric resonator antenna by engraving grooves on its side walls,” *IEEE Antennas Wireless Propag. Lett.*, vol. 16, pp. 2167–2170, 2017.

[15] E. Baldazzi *et al.*, “A high-gain dielectric resonator antenna with plastic-based conical horn for millimeter-wave applications,” *IEEE Antennas Wireless Propag. Lett.*, vol. 19, no. 6, pp. 949–953, Jun. 2020.

[16] S. Fakhte, H. Oraizi, L. Matekovits, and G. Dassano, “Cylindrical anisotropic dielectric resonator antenna with improved gain,” *IEEE Trans. Antennas Propag.*, vol. 65, no. 3, pp. 1404–1409, Mar. 2017.

[17] Y. M. Pan and S. Y. Zheng, “A low-profile stacked dielectric resonator antenna with high-gain and wide bandwidth,” *IEEE Antennas Wireless Propag. Lett.*, vol. 15, pp. 68–71, 2016.

[18] A. Petosa and S. Thirakoune, “Rectangular dielectric resonator antennas with enhanced gain,” *IEEE Trans. Antennas Propag.*, vol. 59, no. 4, pp. 1385–1389, Apr. 2011.

[19] D. Guha, A. Banerjee, C. Kumar, and Y. M. M. Antar, “Higher order mode excitation for high-gain broadside radiation from cylindrical dielectric resonator antennas,” *IEEE Trans. Antennas Propag.*, vol. 60, no. 1, pp. 71–77, Jan. 2012.

[20] D. Guha, A. Banerjee, C. Kumar, and Y. M. M. Antar, “New technique to excite higher-order radiating mode in a cylindrical dielectric resonator antenna,” *IEEE Antennas Wireless Propag. Lett.*, vol. 13, pp. 15–18, 2014.

[21] M. Mrnka and Z. Raida, “Enhanced-gain dielectric resonator antenna based on the combination of higher-order modes,” *IEEE Antennas Wireless Propag. Lett.*, vol. 15, pp. 710–713, 2016.

[22] B. Ahn, H.-W. Jo, J.-S. Yoo, J.-W. Yu, and H. L. Lee, “Pattern reconfigurable high gain spherical dielectric resonator antenna operating on higher order mode,” *IEEE Antennas Wireless Propag. Lett.*, vol. 18, no. 1, pp. 128–132, Jan. 2019.

[23] A. A. Abdulmajid, Y. Khalil, and S. Khamas, “Higher-order-mode circularly polarized two-layer rectangular dielectric resonator antenna,” *IEEE Antenna Wireless Propag. Lett.*, vol. 17, no. 6, pp. 1114–1117, Jun. 2018.

[24] X. Zhang and L. Zhu, “Dual-band high-gain differentially fed circular patch antenna working in TM_{11} and TM_{12} modes,” *IEEE Trans. Antennas Propag.*, vol. 66, no. 6, pp. 3160–3165, Jun. 2018.

[25] X. Zhang, K.-D. Hong, L. Zhu, X.-K. Bi, and T. Yuan, “Wideband differentially fed patch antennas under dual high-order modes for stable high gain,” *IEEE Trans. Antennas Propag.*, vol. 69, no. 1, pp. 508–513, Jan. 2021.

[26] X. Zhang, L. Zhu, and Q.-S. Wu, “Sidelobe-reduced and gain-enhanced square patch antennas with adjustable beamwidth under TM_{03} mode operation,” *IEEE Trans. Antennas Propag.*, vol. 66, no. 4, pp. 1704–1713, Apr. 2018.

[27] T. H. Chang and J. F. Kiang, “Dual-band split dielectric resonator antenna,” *IEEE Trans. Antennas Propag.*, vol. 55, no. 11, pp. 3155–3162, Nov. 2007.